

## Simultaneous inversion of velocity and reflectivity

Yang Yang\*, Jaime Ramos-Martinez, Dan Whitmore, Guanghui Huang and Nizar Chemingui, PGS

### Summary

We introduce an inversion approach to simultaneously invert for both velocity and reflectivity. The core of the inversion workflow is a novel wave-equation that provides the full acoustic wavefield, which is parameterized in terms of velocity and vector reflectivity. A key aspect is the separation of the low- and high-wavenumber components of the gradient based on inverse scattering theory, enabling the sensitivity kernels to update the velocity and the vector reflectivity, respectively. The estimation problem is essentially a multi-parameter inversion where the crosstalk trade-offs between the two parameters are minimized with scale separation. Our adjoint state-based inversion is equivalent to performing Full Waveform Inversion (FWI) and Least-Squares Reverse Time Migration (LS-RTM) using the full acoustic wavefield within the same framework. The final inverted reflectivity is an accurate estimate of the true earth reflectivity, compensated for acquisition and poor illumination effects, and with reduced image crosstalk from multiples. The new approach reduces the turnaround time of imaging projects by combining velocity model building (FWI) and imaging (LS-RTM) into a single inversion process with minimum data preprocessing from an inaccurate initial model. We demonstrate the benefits of our scheme using synthetic and field data examples.

### Introduction

Estimating subsurface velocity is one of the most important problems in exploration geophysics. Over the past decade FWI has emerged as the most promising solution for earth model building. FWI utilizes optimization methods to recover an earth model which generates modeled data that best matches the recorded seismic data. The inversion process is based on mapping the data misfit (difference between modeled and recorded data) to perturbations in the earth model.

In principle, the inversion is capable of recovering a complete earth model with a resolution dictated by the seismic experiment. In practice, and more than three decades after its conception, FWI is still evolving to deliver on that promise. The problem is not the theory itself, but most often a failure by many to recognize seismic inversion as a two-goal process. The earth model can be represented as a smoothly varying (low-wavenumber) velocity macromodel onto which are superimposed sharp contrasts in acoustic properties (high-wavenumber) associated with geological boundaries, expressed as reflectivity. The goals of seismic inversion are to both estimate the velocity and predict the reflectivity without damaging either.

Conventional FWI estimates of the velocity mainly rely on refracted and diving waves that have limited penetration depth. The need to recover velocities in the deep part of the model has triggered a demand for long offset acquisitions that can provide diving waves that penetrate to the required depth. By using sufficient long-offset data and properly handling the cycle-skipping problem, non-linear FWI can recover a good velocity model up to the maximum depth of penetration of the refracted and diving waves. As an alternative, one can utilize reflections to recover velocities in the deep part of the model. By utilizing reflections with the adequate scale separation in the gradient, FWI relaxes this depth limitation and is able to provide velocity updates for deeper structures (e.g., Xu et al., 2012; Zhou et al., 2015).

In theory, the LS-RTM inversion flow is similar to FWI, which also tries to minimize the difference between modeled data and recorded data. Accordingly, it is natural to solve both problems in a joint scheme (e.g., Mora, 1989) where each inversion targets specific wavenumber components. Thus, scale separation in the gradient is essential for minimizing the crosstalk between the two parameters during the inversion. For example, combining both low- and high-wavenumber components in FWI with an inaccurate initial model will lead to incorrect location of the high wavenumber components, which slows down the convergence and increases the probability of being trapped in local minima.

We present a novel seismic inversion approach to simultaneously invert for velocity (FWI) and reflectivity models (LS-RTM). The FWI and LS-RTM loop could be employed alternatively (e.g., Zhou et al., 2015; Chi et al., 2017), but the cost increase is significant. Previously, Berkhout (2012) proposed a joint migration inversion, but this approach uses a modeling engine that prefers waves propagating in the up/down directions. Accordingly, the estimation of the velocity does not consider refracted and diving waves (Verschuur et al., 2016). In our method, we use a full wavefield modeling engine parameterized by velocity and vector reflectivity (Whitmore et al., 2020). The other key element of our scheme is the efficient separation of the low- and high-wavenumber components of the gradient to update velocity and reflectivity, respectively (Whitmore and Crawley, 2012; Ramos-Martinez et al., 2016). With minimal preprocessing of input, the output of this approach is an FWI velocity model that tries to fit the kinematics of refractions, turning waves and reflections and an accurate estimate of the earth reflectivity, which is compensated for acquisition, poor illumination effects and with reduced crosstalk from multiples.

## Simultaneous inversion: FWI + LS-RTM

We first describe the theory supporting the new simultaneous inversion, then we show its performance using a controlled experiment and two field surveys from the Gulf of Mexico and the Campos Basin in Brazil.

### Theory

We use the acoustic wave-equation based on velocity and vector reflectivity as discussed by Whitmore et. al., (2020);

$$\frac{1}{V(\mathbf{x})^2} \frac{\partial^2 P(\mathbf{x}, t)}{\partial t^2} - \nabla^2 P(\mathbf{x}, t) - \frac{\nabla V(\mathbf{x})}{V(\mathbf{x})} \cdot \nabla P(\mathbf{x}, t) + 2\mathbf{R}(\mathbf{x}) \cdot \nabla P(\mathbf{x}, t) = S(\mathbf{x}, t) \quad (1)$$

where  $P$  is the total pressure wavefield which is a function of space ( $\mathbf{x}$ ) and time ( $t$ ),  $V$  is the velocity,  $\mathbf{R}(\mathbf{x}) = \frac{1}{2} \frac{\nabla Z(\mathbf{x})}{Z(\mathbf{x})}$  is the vector reflectivity in which  $Z$  is the impedance and  $S$  is the source. Using this representation, velocity and reflectivity are directly set as the model parameters and there is no need to construct a density model. Also, the modeling procedure is able to generate the full acoustic wavefield, including refracted and reflected energy, as well as free-surface and internal multiples (Whitmore et. al., 2020).

The velocity and the vector reflectivity are updated using their appropriate kernels after scale separation. The velocity kernel (Ramos-Martinez et. al., 2016) is defined as:

$$K_V(\mathbf{x}) = \frac{1}{I(\mathbf{x})} \left[ \int \left( W_1(\mathbf{x}, t) \frac{1}{V(\mathbf{x}, t)^2} \frac{\partial P(\mathbf{x}, t)}{\partial t} \frac{\partial Q(\mathbf{x}, t)}{\partial t} - W_2(\mathbf{x}, t) \nabla P(\mathbf{x}, t) \cdot \nabla Q(\mathbf{x}, t) \right) dt \right], \quad (2)$$

and the impedance kernel (Whitmore and Crawley, 2012) used for migration is defined as:

$$K_Z(\mathbf{x}) = \frac{1}{I(\mathbf{x})} \left[ \int \left( W_3(\mathbf{x}, t) \frac{1}{V(\mathbf{x}, t)^2} \frac{\partial P(\mathbf{x}, t)}{\partial t} \frac{\partial Q(\mathbf{x}, t)}{\partial t} + W_4(\mathbf{x}, t) \nabla P(\mathbf{x}, t) \cdot \nabla Q(\mathbf{x}, t) \right) dt \right], \quad (3)$$

where  $W_i$  ( $i = 1, 2, 3, 4$ ) are dynamic weights,  $P$  and  $Q$  are the forward and adjoint wavefields and  $I$  is the illumination term. The inversion scheme updates both velocity and reflectivity during each iteration. By carefully choosing  $W_i$ , larger scattering contribution can be gradually added into the velocity kernel to enrich the wavenumber spectrum while minimizing the crosstalk between the two parameters (e.g., Luo and Wu, 2018). If reflectivity is not updated, the flow reduces to an FWI procedure to update the velocity model (e.g., Yang et. al., 2020). If only the impedance kernel is used, the workflow is then similar to LS-RTM.

### Synthetic example

We use a modified version of the SEG overthrust model to demonstrate the benefits of our joint inversion scheme. We simulate the input data by solving the variable density wave-equation, from the true velocity (Figure 1a) and density models (Figure 1b). The density model is calculated using Gardner's equation based on the true velocity model. We compute the true vertical reflectivity (Figures 1d) from the true velocity and density models. For the initial models, we consider a smoothed version of the true model and zero reflectivity. The source function is an Ormsby filtered spike with corner frequencies of 3-5-20-35 Hz. The maximum

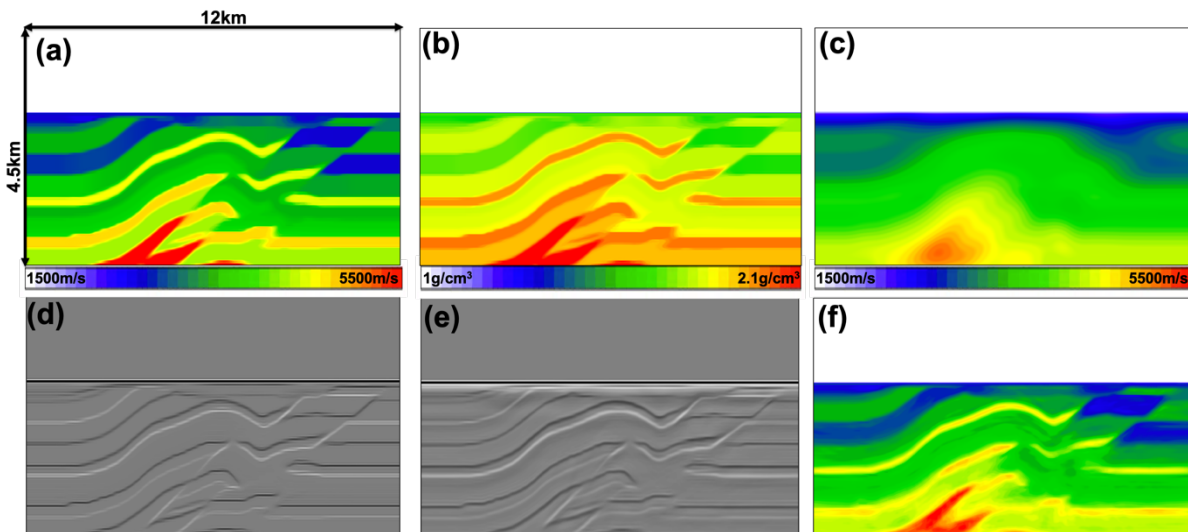


Figure 1: Overthrust model synthetic test example. True velocity (a) and density (b) model. (c) Initial velocity model. (d) True vertical reflectivity. (e) Inverted vertical reflectivity and (f) velocity from the simultaneous inversion.

## Simultaneous inversion: FWI + LS-RTM

offset used is 4 km, thus the inversion is mostly driven by reflections. In Figures 1e and 1f, the results of the joint velocity and vector reflectivity are displayed. The inverted velocity from our joint inversion correctly retrieves detailed features associated with the velocity model. Similarly, the inverted vertical reflectivity is a good estimate of the true vertical reflectivity. All components of vector reflectivity are used in the inversion although we only display the vertical component in Figure 1.

### Field data examples

We illustrate the benefits of our new simultaneous inversion using two field datasets acquired with multisensor streamers. In both examples, we start from simple initial models and use the total pressure field with minimum pre-processing and a maximum full power frequency of 20 Hz. The kinematics of the initial model are not accurate but no cycle skipping is observed at the selected frequency band.

The first field data example corresponds to data acquired in deep water Gulf of Mexico (Desoto Canyon area). The maximum offset is 12 km. Figure 2a shows the initial velocity model while the initial reflectivity is assumed to be

zero. In Figure 2c, we show the reflectivity from the first iteration of the inversion, which is equivalent to performing RTM with the initial model but using data with ghost effects. In this first image, the crosstalk produced by the multiple energy from the unconformity interfering with the deep reflections is indicated by the oval. The results after several iterations of the joint inversion are shown in Figures 2b and 2d. Finer details are present in the inverted velocity model. Also, notice coherency enhancement and clear reduction of the crosstalk in the final reflectivity model.

The second field data example corresponds to a deep water setting in offshore Brazil (Campos basin). The maximum inline offset acquired in this survey is 10 km. In Figures 3a and 3b, we show the reflectivity model for one inline at the first iteration and final inversion, respectively. Velocity updates are displayed in Figure 3c. Note the improvement in the resolution of the shallow fault system (yellow ovals). Moreover, there is a coherency enhancement in the deep reflectors of the mini-basin and in the salt flanks (yellow arrows). These observations are supported by the image gathers computed for the initial and the final FWI model from the joint inversion, which are shown in Figures 3d and 3e, respectively. Finally, a depth slice at 3.4 km of the initial

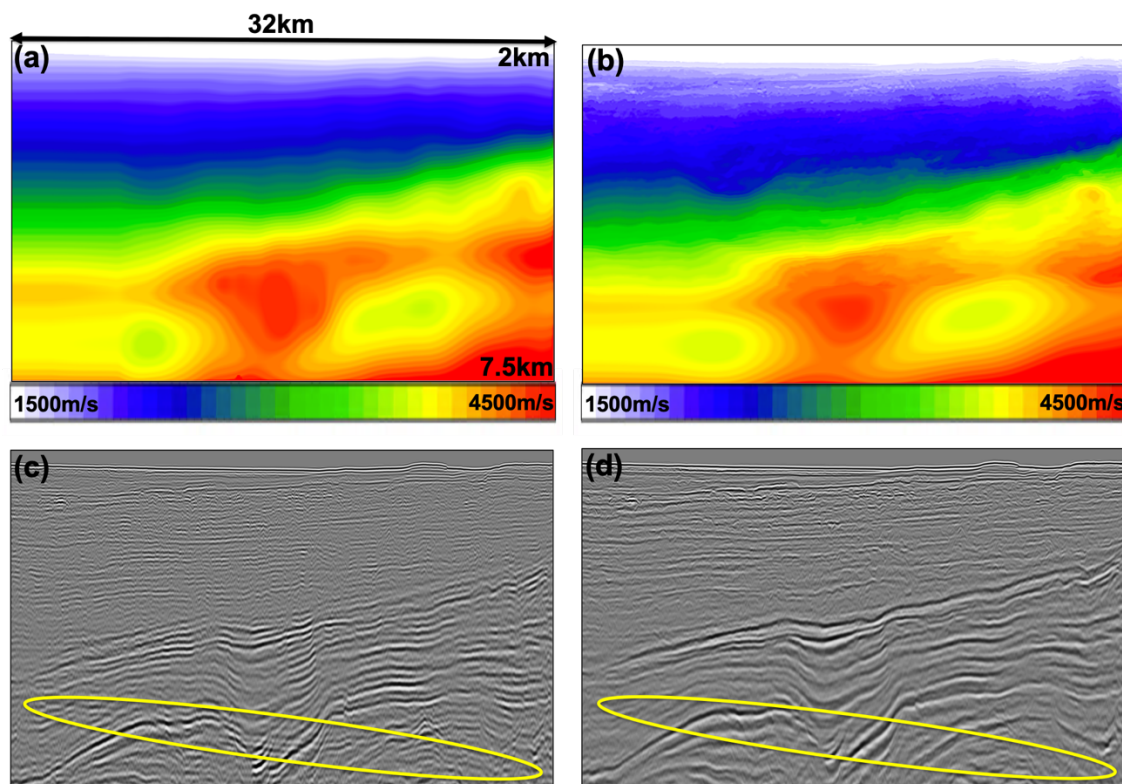


Figure 2: Desoto Canyon field data example. (a) Initial and (b) inverted velocity models. (c) Vertical reflectivity from first iteration. (d) Final inverted vertical reflectivity. Notice the crosstalk reduction as the yellow oval indicates.

### Simultaneous inversion: FWI + LS-RTM

velocity model (Figure 3f) is compared with the final FWI model (Figure 3g). Note the enhanced spatial resolution and the detailed features in the FWI model that are conformable to the structure.

#### Conclusions

We present a new seismic inversion workflow to simultaneously estimate the earth reflectivity and velocity models. At the heart of the inversion workflow is a wave-equation modeling procedure using vector reflectivity to compute the predicted velocity and reflectivity models. Using inverse scattering theory, the low- and high-wavenumber components of the gradient are effectively separated and the velocity and the reflectivity are updated respectively. We successfully applied our workflow to two

field data examples. Results demonstrated that our inversion is able to retrieve an accurate representation of the earth reflectivity, which is more correctly positioned, compensated for acquisition and poor illumination, and with reduced image crosstalk from multiples. We demonstrate that FWI and LS-RTM can be realized simultaneously as a single inversion workflow, with significant reduction in turnaround time for the model building and imaging project.

#### Acknowledgments

We thank Tiago Alcantara for his assistance in the field data example. We thank PGS for the authorization to publish this work.

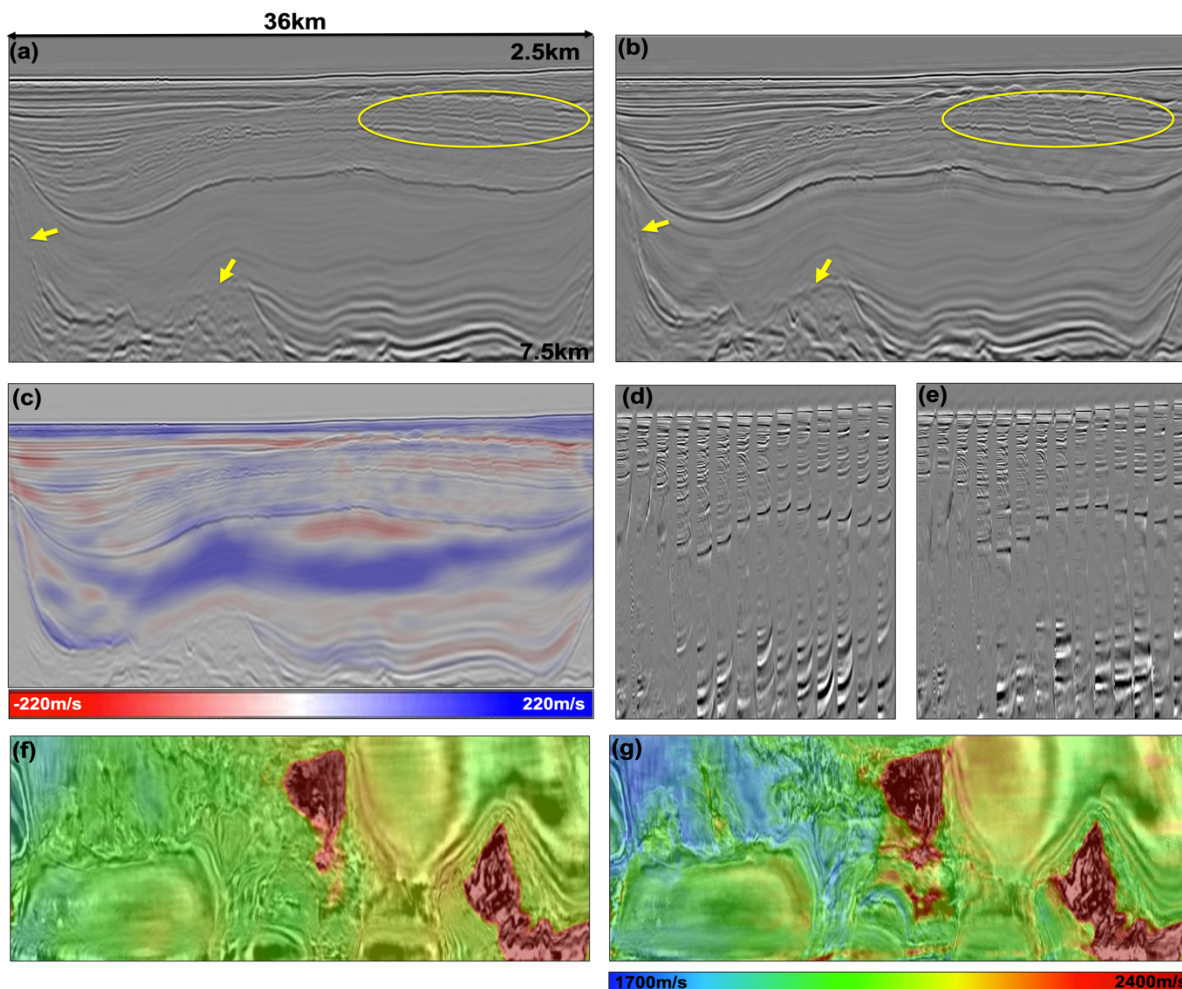


Figure 3: Campos Basin field data example. (a) Vertical reflectivity from first iteration. (b) Final inverted vertical reflectivity. (c) Velocity updates on final vertical reflectivity. Image gathers from the initial model (d) and the FWI model (e). (f) Depth slice of the initial velocity at 3.4 km plotted on top of the first iteration of reflectivity inversion. (g) Depth slice of the FWI model on the final inverted reflectivity.

## References

- Berkhout, A. J., 2012, Combining full wavefield migration and full waveform inversion, a glance into the future of seismic imaging: *Geophysics*, **77**, no. 2, S43–S50, doi: <https://doi.org/10.1190/geo2011-0148.1>.
- Chi, B., K. Gao, and L. Huang, 2017, Least-squares reverse time migration guided full-waveform inversion: 2017 SEG Technical Program, Expanded Abstract, 1471–1475, doi: <https://doi.org/10.1190/segam2017-17775494.1>.
- Luo, J., and R. S. Wu, 2018, Velocity and density reconstruction based on scattering angle separation: *Pure and Applied Geophysics*, **175**, 4371–4387, doi: <https://doi.org/10.1007/s00024-018-1916-8>.
- Mora, P., 1989, Inversion = migration + tomography: *Geophysics*, **54**, no. 12, 1575–1586, doi: <https://doi.org/10.1190/1.1442625>.
- Ramos-Martinez, J., S. Crawley, K. Zou, A. A. Valenciano, L. Qiu, and N. Chemingui, 2016, A robust gradient for long wavelength FWI updates: 78th EAGE Conference & Exhibition, Extended Abstracts, 1–5, doi: <https://doi.org/10.3997/2214-4609.201601536>.
- Verschuur, D. J., X. R. Staal, and A. J. Berkhout, 2016, Joint migration inversion: Simultaneous determination of velocity fields and depth images using all orders of scattering: *The Leading Edge*, **35**, 1037–1046, doi: <https://doi.org/10.1190/tle35121037.1>.
- Whitmore, N. D., J. Ramos-Martinez, Y. Yang, and A. A. Valenciano, 2020, Full wave field modeling with vector- reflectivity: 82nd EAGE Conference & Exhibition, Extended Abstracts.
- Whitmore, N. D., and S. Crawley, 2012, Application of RTM inverse scattering imaging conditions: 2012 SEG Technical Program, Expanded Abstracts, 1–6, doi: <https://doi.org/10.1190/segam2012-0779.1>.
- Xu, S., D. Wang, F. Chen, Y. Zhang, and G. Lambaré, 2012, Full waveform inversion for reflected seismic data: 74th Annual International Conference and Exhibition, Extended Abstracts, doi: <https://doi.org/10.3997/2214-4609.20148725>.
- Yang, Y., J. Ramos-Martinez, D. Whitmore, A. A. Valenciano, and N. Chemingui, 2020, Full waveform inversion using wave equation reflectivity modeling: 82nd EAGE Annual Conference & Exhibition, Extended Abstracts, 1–5, doi: <https://doi.org/10.3997/2214-4609.202011146>.
- Zhou, W., R. Brossier, S. Operto, and J. Virieux, 2015, Full waveform inversion of diving and reflected waves for velocity model building with impedance inversion based on scale separation, *Geophysical Journal International*, **202**, 1535–1554, doi: <https://doi.org/10.1093/gji/ggv228>.